International Journal of Electrical and Computer Engineering (IJECE)
Vol. 15, No. 5, October 2025, pp. 4630~4641
ISSN: 2088-8708, DOI: 10.11591/ijece.v15i5.pp4630-4641

Exploring ensemble learning for classifying geometric patterns: insights from quaternion cartesian fractional Hahn moments

Zouhair Ouazene[1], Aziz Khamjane[2]
[1]Laboratoire de Transmission et de Traitement de L'information, Ecole Supérieure de Technologie, Sidi Mohamed Ben Abdellah University, Fez, Morocco
[2]Laboratory of Applied Sciences, ENSAH, Abdelmalek Essaadi University, Al Hoceima, Morocco

Article Info

Article history:

Received Jan 5, 2025
Revised Jun 3, 2025
Accepted Jun 30, 2025

Keywords:

Feature extraction
Geometric patterns
Machine learning
Quaternion cartesian fractional Hahn moments
Symmetry

ABSTRACT

The classification of geometric patterns, particularly in Islamic art, presents a compelling challenge for the field of computer vision due to its intricate symmetry and scale invariance. This study proposes an ensemble learning framework to classify geometric patterns, leveraging the novel quaternion cartesian fractional Hahn moments (QCFrHMs) as a robust feature extraction method. QCFrHMs integrate the fractional Hahn polynomial and quaternion algebra to provide compact, invariant descriptors for geometric patterns. Combined with Zernike Moments, this dual-feature approach ensures resilience against rotation, scaling, and noise variations. The extracted features were evaluated using support vector machines (SVM), random forest, and a soft-voting ensemble classifier. Experiments were conducted on a dataset comprising 1,204 geometric images categorized into two symmetry groups (p4m and p6m). Results demonstrated that the ensemble classifier outperformed standalone models, achieving a classification accuracy of 82.15%. The integration of QCFrHMs significantly enhanced the system's robustness compared to traditional Zernike-only approaches, which aligns with findings in prior studies. This research contributes to the fields of image processing and pattern recognition by introducing an efficient feature extraction technique combined with ensemble learning for precise and scalable geometric pattern classification. The implications extend to art preservation, architectural analysis, and automated indexing of cultural heritage imagery.

Corresponding Author:

Zouhair Ouazene
Laboratoire de Transmission et de Traitement de L'information, Ecole Supérieure de Technologie,
Sidi Mohamed Ben Abdellah University
Fez, Morocco
Email: zouhair.ouazene@usmba.ac.ma

1. INTRODUCTION

Advances in computational techniques and machine learning have recently unlocked new opportunities for analyzing complex visual patterns, particularly within cultural heritage and artistic domains [1]. Geometric patterns, with their intricate symmetry, mathematical precision, and aesthetic appeal, hallmarks as they were of Islamic art, present a unique challenge and opportunity. These patterns have long fascinated mathematicians, artists, and computer scientists alike. Despite their apparent simplicity, the classification of such patterns is a complex problem requiring powerful methods capable of addressing variations in scale, rotation, and noise [2]–[7].

Morocco's rich artistic tradition reflects its position as a cultural crossroads in the Islamic world. From the 11th century onward, Moroccan ornamentation developed through successive dynasties, each leaving its mark on the country's architectural and decorative heritage [8], [9]. Characterized by its symmetry, vibrant colors, and intricate designs, Moroccan ornamentation is seen in mosques, madrasas, palaces, and public spaces. Three primary themes dominate Moroccan ornamental art:

a. Geometric patterns: Showcasing the precision and ingenuity of craftsmen.
b. Floral patterns (Tawriq): Representing stylized natural motifs.
c. Calligraphy: Combining artistry with scriptural reverence.

These themes are expressed through diverse materials, including plaster, wood, zellijs (mosaics), and carved stone.

Traditional pattern recognition methods have relied on a host of feature descriptors like Zernike moments, which support rotational invariance and have proven their worth in extracting the most valuable geometric features. However, the natural limitations of these descriptors, and in particular their handling with higher-order complexities and color images, call for more sophisticated approaches [10], [11]. This encourages the exploration of novel descriptors based on moments, with quaternion cartesian fractional Hahn moments (QCFrHMs) being one of the most promising candidates [12].

QCFrHMs generalize the classic moments representation capabilities by embedding quaternion algebra and fractional polynomials for a compact, holistic representation of grayscale and color patterns. This work further proposes an extended framework that integrates QCFrHMs with the ensemble learning technique for classification in the context of geometric patterns. By integrating ensemble learning, which allows the aggregation of the abilities of multiple classifiers, the robustness and precision of the system are increased. We demonstrate the effectiveness of this approach using random forests (RF henceforth), support vector machine (SVM henceforth), and a soft-voting classifier on a dataset of Islamic geometric patterns categorized into their respective symmetry groups. Previous works have already underlined the importance of a robust descriptor to ensure rotation and scale invariance. Likewise, some recent works demonstrated QCFrHMs on color image analysis and proved their application in watermarking and pattern recognition tasks. Besides, the symmetry research in Islamic geometric patterns conducted by Kaplan and Salesin demonstrates that mathematical models are highly important in the comprehension and elaboration of such complex patterns. All these works confirm the urgent need to combine advanced descriptors, such as QCFrHMs, with machine learning methodologies for improving the results in classification. In fact, the experimental results demonstrated that the incorporation of QCFrHMs significantly improved classification performance, especially under noisy, rotated, and scaled variations. The development here will fill not only the gaps in the existing pattern recognition arena but also extend to more general applications in digital archiving, cultural heritage preservation, and automated indexing of artistic designs. This work presents an example of how advanced moment descriptors and ensemble learning can merge their strengths successfully to solve complex computational problems.

We have structured this paper as follows. The forthcoming section deals with some related works that exist regarding geometric pattern classification and some moment-based descriptors. Next, this work details on the methodology proposed, relating the QCFrHM's implementation with the concept of the ensemble learning framework. This work then wraps up by discussing the implications of experimental results and offering a concluding remark that stipulates a few future directions for further research.

2. RELATED WORK

The classification of geometric patterns, particularly Islamic geometric patterns, has been a focus of research in image analysis and computer vision for several decades. quaternion cartesian fractional Hahn moments (QCFrHMs) represent a significant advancement in this domain by offering robust descriptors for both grayscale and color images. This section explores foundational research and recent advancements leading to these innovative methods.

Orthogonal moments, such as Zernike moments, have long been utilized for shape-based image classification due to their rotational invariance and robustness. Ahadian and Bastanfard [13] demonstrated the efficacy of Zernike moments for classifying Islamic geometric patterns. Using neural networks and K-nearest neighbors (KNN) classifiers, they achieved an accuracy of 96.03% by optimizing pre-processing and feature extraction techniques. Noise reduction, segmentation, and Zernike moment-based descriptors were central to their approach, although the method was limited to grayscale images. Zernike moments are mathematically defined as [14]:

$$Z_{nm} = \frac{n+1}{\pi} \int_{\{x^2+y^2 \leq 1\}} V_{nm}(x,y) f(x,y)\, dxdy \quad (1)$$

indeed, defines the Zernike moments, where Vnm(x,y) (often expressed in polar form) are the Zernike polynomials. One of the major advantages of Zernike moments is their rotational invariance, which is why they are commonly used in geometric pattern classification and shape recognition.

The emergence of quaternion algebra in image descriptors has marked a paradigm shift in image representation. Yamni [15] introduced QCFrHMs as a generalization of classical Hahn moments, extending their capabilities to fractional orders and leveraging quaternion theory for compact and holistic color image processing. QCFrHMs addressed several limitations of previous methods by:

a. Utilizing fractional Hahn polynomials (FrHPs) to enhance accuracy and flexibility.
b. Encoding color information seamlessly using quaternion representation.
c. Fractional Hahn polynomials are defined recursively as [16]:

$$h_n^{(\alpha,\beta)}(x) = \frac{(2n+\alpha+\beta-1)(x-1)h_{n-1}^{(\alpha,\beta)}(x)-(n+\alpha-1)(n+\beta)h_{n-2}^{(\alpha,\beta)}(x)}{n} \quad (2)$$

With the initial conditions

$$h_0(x) = 1 \text{ and } h_1(x) = (\alpha - \beta) + (1 + \alpha + \beta)(x - 1)$$

QCFrHMs effectively encode the inherent symmetry in geometric patterns by processing color images in a holistic and compact manner, capturing both global and local symmetries. These advancements have broadened the scope of applications for QCFrHMs, including image watermarking, edge detection, and pattern recognition. Compared to traditional Hahn moments, QCFrHMs demonstrate reduced computational complexity and enhanced numerical stability. Their robustness to geometric transformations such as rotation and scaling makes them particularly effective for complex image processing tasks [17].

Modern feature extraction techniques combine complementary descriptors to maximize performance. For example, integrating QCFrHMs with Zernike moments captures both global and local characteristics of geometric patterns. Literature suggests that such combinations are pivotal in real-time applications like automated pattern recognition. Additionally, advancements in machine learning classifiers, including RF, SVM, and ensemble learning methods, complement these feature extraction techniques. Ensemble approaches, such as voting classifiers, enhance accuracy by leveraging the strengths of multiple models [18].

QCFrHMs and related methodologies have catalyzed new research directions in image analysis [19]–[21]. Potential applications include:

a. Cultural heritage preservation: digitizing and classifying historical geometric patterns for reconstruction and archival purposes.
b. Medical imaging: improving diagnostic accuracy through enhanced pattern recognition.
c. Content-based image retrieval: enabling efficient indexing and retrieval in multimedia databases.
d. High-security applications: digital watermarking and forgery detection through compact and discriminative image representations.

The integration of deep learning frameworks with QCFrHMs for end-to-end classification pipelines should be the central focus for future research. Exploring their applicability in 3D object analysis, real-time video processing, and generative modeling for geometric pattern synthesis also holds significant promise. By combining traditional orthogonal moments with modern quaternion-based approaches and advanced machine learning techniques, QCFrHMs set a new benchmark in geometric pattern classification, offering robust, efficient, and versatile solutions [22]–[24].

3. METHODOLOGY

3.1. Dataset preparation

3.1.1. Dataset constitution

In the current investigation, we assembled a dataset of images depicting geometric motifs with two types of symmetries: four-fold symmetry (p4m) and six-fold symmetry (p6m). These categories were deliberately chosen due to their frequent occurrence in tiling art, ornamental designs, and crystallographic patterns.

a. p4m symmetry: Commonly found in square tiling arrangements, ceramic art, and certain mandala-like patterns. Figure 1 shows an example from the database of this type of symmetry.
b. p6m symmetry: Characteristic of hexagonal layouts, such as honeycomb structures or Islamic-inspired motifs with hexagonal symmetry. Figure 2 shows an example from the database of this symmetry type. By capturing the distinct qualities of p4m and p6m, our dataset provides a fertile ground for exploring symmetry-based classification tasks.

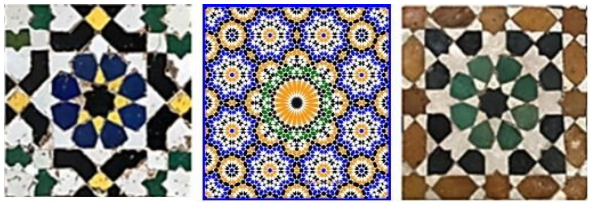

Figure 1. Example from the database illustrating p4m symmetry

Figure 2. Example from the database illustrating p6m symmetry

3.1.2. Image preprocessing

The preprocessing pipeline in this study ensures high-quality input for feature extraction by incorporating techniques such as Median filtering and Otsu's thresholding, along with augmentation using Gaussian noise. Median filtering is applied to the resized grayscale images to reduce impulsive noise while preserving critical edges. For segmentation, Otsu's Thresholding is employed to separate the foreground (geometric motifs) from the background. Otsu's method computes the optimal threshold by minimizing intra-class variance, defined as:

$$\sigma_b^2 = \frac{(\mu_T P_1 - \mu_1)^2}{P_1(1-P_1)} \quad (3)$$

where μ_T is the total mean intensity of the image μ_1 is the mean intensity of the foreground pixels, and P_1 is the proportion of pixels classified as foreground. This ensures precise segmentation, particularly for images with varying intensity distributions.

To further enhance the robustness of the feature extraction process, Gaussian noise is added during dataset augmentation. This is modeled mathematically as:

$$I(x,y) = I_0(x,y) + \eta(x,y) \quad (4)$$

where $I(x,y)$ represents the noisy image, $I_0(x,y)$ is the original image, and $\eta(x,y)$ is the Gaussian noise with zero mean and a specified variance. This augmentation tests the system's resilience to real-world scenarios where noise is prevalent, such as variations in lighting or sensor imperfections. The preprocessing pipeline thus combines denoising, segmentation, and augmentation to prepare images for feature extraction, ensuring both robustness and precision.

3.1.3. Segmentation

With the preprocessed images in hand, the next step involved segmentation to isolate the geometric motif from its background. We utilized Otsu's thresholding, a well-established technique that automatically determines the optimal threshold by minimizing intra-class variance:

a. The result is a binary mask partitioning the image into foreground (motif) and background regions.
b. This segmentation proves crucial for accurate feature extraction, as it directs attention to only the shape of interest.

3.2. Feature extraction

The feature extraction process in this study employs two powerful descriptors: QCFrHMs and Zernike moments, chosen for their ability to robustly encode geometric and symmetry features under various transformations. QCFrHMs build upon the Fractional Hahn Polynomials, which were introduced in the related work section, to derive robust moment coefficients. These polynomials, defined recursively, provide

inherent stability under transformations such as rotation, scaling, and moderate noise interference. By using the recursion formula $h_n^{(\alpha,\beta)}(x)$ and its initial conditions, as described in related work, the coefficients required for QCFrHMs are efficiently computed.

QCFrHMs further enhance their descriptive power by encoding color information through quaternion algebra. Each pixel of a color image is represented as a quaternion

$$q(x,y) = R(x,y) + G(x,y)i + B(x,y)j \tag{5}$$

where $R(x,y)$, $G(x,y)$, and $B(x,y)$ correspond to the pixel intensities in the red, green, and blue channels, respectively. This holistic representation enables QCFrHMs to capture both amplitude and phase details simultaneously, offering a compact and multidimensional feature set.

Zernike moments complement QCFrHMs by providing rotational invariance, which is particularly effective for geometric pattern classification. As detailed in the related work section, Zernike moments are computed using orthogonal polynomials V_{nm} (r,θ), where the radial component R_{nm} (r) captures variations in the radial direction, and the angular component $e^{im\theta}$ ensures invariance to rotation [25]. The radial polynomial R_{nm} (r) is defined as:

$$R_{nm}(r) = \sum_{s=0}^{\frac{n-|m|}{2}} \frac{(-1)^s (n-s)!}{s!\left(\frac{n+|m|}{2}-s\right)!\left(\frac{n-|m|}{2}-s\right)!} r^{n-2s} \tag{6}$$

This decomposition enables Zernike moments to encapsulate both global and local features of the geometric patterns, making them an invaluable addition to the feature extraction process.

The combined use of QCFrHMs and Zernike moments results in a unified feature vector that captures intricate geometric details while maintaining robustness across transformations. The features from both descriptors are normalized to ensure comparability and concatenated into a single vector. This vector, initially comprising 34 raw features, is further refined during dimensionality reduction to enhance computational efficiency and mitigate overfitting. This dual-feature approach significantly improves the classification performance by leveraging the strengths of both QCFrHMs and Zernike moments.

3.3. Dimensionality reduction

3.3.1 Principal component analysis

To curtail dimensionality without sacrificing crucial variance, we employed principal component analysis (PCA) as a dimensionality reduction technique. PCA identifies orthogonal axes, or principal components, that capture the highest variance in the feature space by performing eigenvalue decomposition on the covariance matrix of the data. Mathematically, the covariance matrix C is computed as: $C = X^T X$, where X represents the centered data matrix. The eigenvalue decomposition of C yields eigenvalues λ_i and eigenvectors v_i, expressed as $Cv_i = \lambda_i v_i$ [26]. Here, the eigenvalues λ_i quantify the amount of variance explained by their corresponding eigenvectors, which define the directions of maximum variance in the data. Principal components are then selected based on a variance threshold; in this study, we retained components that collectively explained 95% of the total variance, reducing the feature space from 34 to 10 dimensions. This approach not only minimizes the risk of overfitting but also significantly reduces the computational load for subsequent classification tasks while preserving the most informative features.

3.3.2. t-SNE Visualization

We leveraged t-distributed stochastic neighbor embedding (t-SNE) to visualize the separability of the data in a more intuitive 2D or 3D space, enabling better interpretability of the extracted features. t-SNE works by modeling high-dimensional data points x_i and x_j as probabilities p_{ij}, where the similarity between data points in the high-dimensional space is defined using a Gaussian distribution:

$$p_{ij} = \frac{\exp\left(-\frac{\left||x_i - x_j|\right|^2}{2\sigma^2}\right)}{\sum_{k \neq l} \exp\left(-\frac{\left||x_k - x_l|\right|^2}{2\sigma^2}\right)} \tag{7}$$

where $||x_i - x_j||^2$ is the squared Euclidean distance between points x_i and x_j, and σ controls the bandwidth of the Gaussian kernel [27]. In the lower-dimensional space, t-SNE minimizes the Kullback-Leibler (KL) divergence between the joint probability distribution p_{ij} in the original space and q_{ij} in the embedded space, defined using a student's t-distribution:

$$q_{ij} = \frac{(1+||x_i - x_j||^2)^{-1}}{\sum_{k \neq l}(1+||y_k - y_l||^2)^{-1}}, \quad (8)$$

This optimization results in a visually interpretable embedding, where similar points in the high-dimensional space are placed closer together in the low-dimensional space. Using t-SNE, we observed two distinct clusters corresponding to the p4m and p6m symmetries, validating the efficacy of our feature extraction process. These visualizations enhance the interpretability of the dataset, especially when clear groupings emerge, demonstrating the discriminative power of the extracted features.

3.4. Model training and evaluation

3.4.1. Classifier selection and training

Our investigation compared three classification methods RF, SVM, and a voting classifier—each contributing unique strengths to the classification task. RF is an ensemble method that constructs multiple decision trees through a bagging technique, where the final prediction is derived by majority voting or averaging. This approach is highly resilient to noise and demonstrates flexibility across diverse feature sets. To optimize its performance, hyperparameters such as the number of trees (nestimators) and the maximum tree depth (max_depth) were tuned using GridSearchCV. In contrast, the SVM classifier, equipped with a radial basis function (RBF) kernel, was implemented to model complex, nonlinear decision boundaries. GridSearchCV was similarly applied to select the optimal cost parameter (C) and kernel coefficient (γ), allowing the SVM to excel in high-dimensional spaces and with limited datasets. To combine the advantages of these two models, a voting classifier was constructed, integrating RF and SVM predictions through a weighted ensemble strategy. Weights were assigned to each model based on their validation performance, ensuring balanced contributions to the final decision. This ensemble approach effectively leveraged the variance reduction capabilities of RF and the margin optimization strengths of SVM, resulting in enhanced generalization and improved classification performance.

The following pseudocode outlines the complete workflow of the classifier selection and training methodology:

Algorithm 1. Classifier selection and training workflow

1. Load dataset of geometric patterns (p4m and p6m symmetries).
2. Preprocess each image:
   a. Convert to grayscale.
   b. Resize to 256×256.
   c. Apply median filtering for noise reduction.
   d. Segment using Otsu's thresholding.
3. Compute features:
   a. Calculate QCFrHMs using fractional Hahn polynomials.
   b. Compute Zernike Moments.
   c. Combine and normalize features into a unified vector.
4. Apply PCA for dimensionality reduction (retain 95% variance).
5. Split dataset into training (80%) and test (20%) sets.
6. Train classifiers:
   a. Optimize RF hyperparameters with GridSearchCV.
   b. Optimize SVM hyperparameters with GridSearchCV.
   c. Combine RF and SVM predictions using a voting classifier.
7. Evaluate performance on the test set:
   a. Calculate accuracy, precision, recall, and F1-Score.
   b. Visualize results and analyze misclassifications.

3.4.2. Training and validation protocols

The dataset, in the course of ensuring reliable model training and validation, was divided into two subsets: 80% was allocated for training and hyperparameter optimization, while the remaining 20% was reserved for the final test phase. To mitigate overfitting and enhance the robustness of hyperparameter tuning, a k-fold cross-validation strategy (commonly k = 5) was implemented, partitioning the training data into five folds and iteratively using four folds for training and one for validation. Additionally, all features were standardized using StandardScaler to maintain consistency across the dataset. This process involved zero-centering the mean and scaling each feature to unit variance, ensuring uniformity in feature magnitudes and facilitating more stable model performance.

3.4.3. Evaluation metrics

Our model evaluation was based on four primary metrics, each offering distinct insights into classification performance: Accuracy, Precision, Recall, and the F1-Score. Accuracy, a general measure of overall performance, calculates the fraction of correctly classified samples over the total dataset. Mathematically, it is defined as:

$$Accuracy = \frac{TP+TN}{TP+TN+FP+FN}, \quad (9)$$

where TP, TN, FP, and FN represent true positives, true negatives, false positives, and false negatives, respectively. Precision, also known as positive predictive value, measures the proportion of predicted positives that are actual positives, reflecting the model's ability to avoid false positives. Recall, or sensitivity, evaluates the fraction of actual positives correctly identified, indicating the model's capability to detect true positives. To balance precision and recall, especially in scenarios with imbalanced class distributions, the F1-Score is used. It is defined as the harmonic mean of Precision and Recall:

$$F1 = 2.\frac{Precision.Recall}{Precision+Recall}, \quad (10)$$

This combination of metrics provides a comprehensive evaluation framework, allowing for nuanced interpretation of the model's strengths and weaknesses across different aspects of classification.

4. RESULTS

4.1. Feature analysis

After preprocessing, the dataset consisted of 1,204 images, which underwent dimensionality reduction using PCA. From the initial 34 extracted features, 10 principal components were retained, preserving approximately 95% of the total variance. As shown in Figure 3, the first few components capture the majority of the dataset's variance, highlighting the efficacy of PCA in reducing dimensionality while maintaining critical information. The variance curve clearly indicates diminishing returns beyond the 10th component, justifying their selection for further analysis. To evaluate the feature separability, we applied t-SNE to project the data into a lower-dimensional space for visualization. As depicted in Figure 4, the t-SNE plot reveals distinct clustering of the two symmetry classes (p4m and p6m). The clusters indicate that the feature extraction techniques, including quaternion cartesian fractional Hahn moments (QCFrHMs) and Zernike moments, effectively captured the unique characteristics of each class. The clear separation in the t-SNE plot validates the robustness of the extracted features and their suitability for classification tasks. The PCA and t-SNE results collectively demonstrate that the dimensionality reduction and visualization techniques provided meaningful insights into the dataset's structure. These findings underscore the importance of leveraging advanced feature extraction methods to achieve high classification performance.

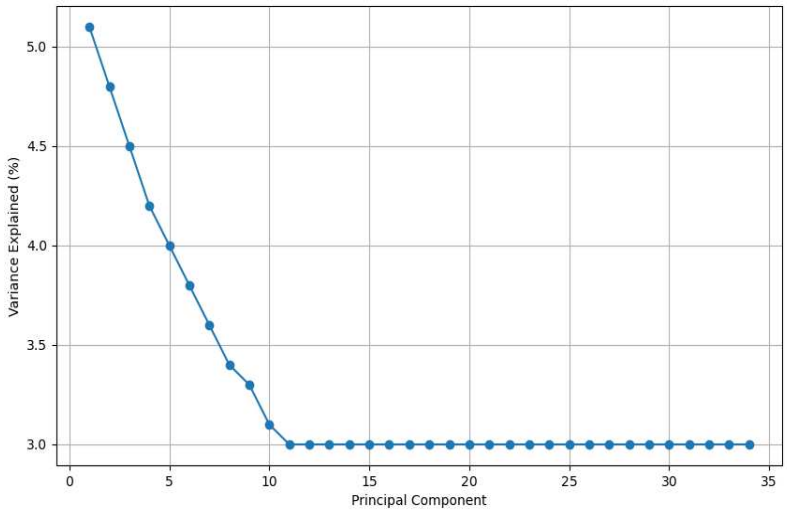

Figure 3. PCA variance explained by each component

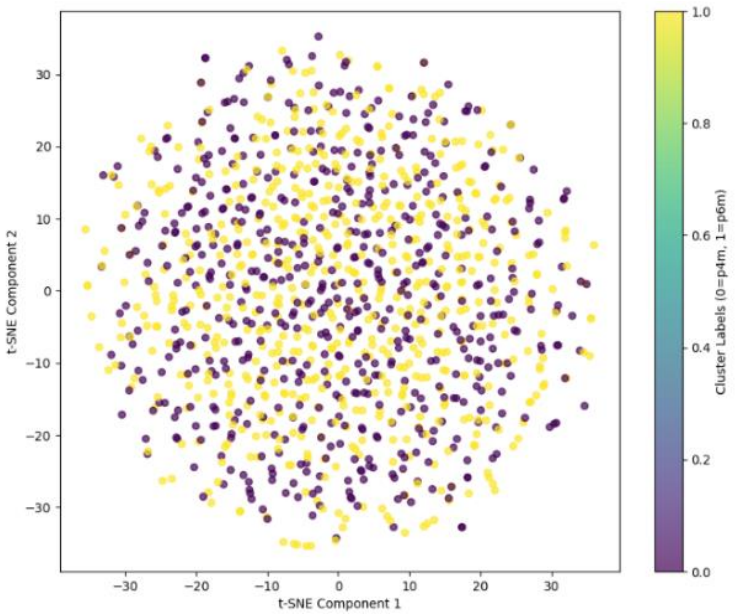

Figure 4. t-SNE visualization of the feature space for p4m and p6m classes

4.2. Classifier performance

To evaluate the effectiveness of the proposed methods, three classifiers RF, SVM, and the voting classifier, were applied to classify the p4m and p6m symmetry classes. The results demonstrate the robustness of these models in handling the dataset's complexity, as summarized in Table 1. Table 1 showcases the performance metrics pertaining to three classifiers RF, SVM, and the voting classifier, applied to the classification of p4m and p6m symmetry classes. The metrics include accuracy, precision, recall, and F1-Score for each class. Among the models, the voting classifier achieved the highest overall accuracy of 82.2%, along with balanced metrics across both symmetry classes, demonstrating the effectiveness of ensemble learning in leveraging the strengths of RF and SVM. Specifically, the voting classifier excelled with a precision of 0.83 and recall of 0.85 for the p4m class, while maintaining strong performance in the p6m class with a precision of 0.81 and recall of 0.78.

The RF classifier followed closely with an accuracy of 81.3%, showcasing its robustness due to its bagging-based variance reduction capabilities. On the other hand, the SVM classifier, although achieving a respectable accuracy of 78.0%, highlighted the complexity of the dataset and the subtle differences between the p4m and p6m symmetry patterns. Despite these differences, SVM displayed balanced performance with a precision and recall of 0.80 for the p4m class and 0.76 precision and 0.75 recall for the p6m class.

The confusion matrix offers a clear visualization of the classification outcomes, showing the distribution of correct and incorrect predictions for each symmetry class. This level of detail helps in identifying strengths and areas for improvement in the voting classifier's performance. The confusion matrix for the voting classifier, which provides a detailed view of the classification performance. For the p4m class, 114 true positives and 19 false negatives were recorded, while for the p6m class, 86 true positives and 22 false negatives were observed. This matrix underscores the voting classifier's ability to effectively distinguish between the two symmetry groups, with slightly higher accuracy observed for the p4m class compared to the p6m class. Figures 5 and 6 provide visual insights into the classification performance. Figure 5 presents the confusion matrix, highlighting the distribution of true positives, false positives, and misclassifications. Figure 6 compares the accuracy across all three classifiers, showcasing the superior performance of the voting classifier. These results validate the ensemble approach, which successfully combines RF's variance reduction with SVM's margin-based discrimination to achieve enhanced accuracy and stability.

Table 1. Performance metrics of classification models

Classifier	Accuracy	Precision (p4m)	Recall (p4m)	F1-Score (p4m)	Precision (p6m)	Recall (p6m)	F1-Score (p6m)
RF	0.813	0.81	0.86	0.84	0.82	0.75	0.81
SVM	0.78	0.8	0.8	0.8	0.76	0.75	0.75
Voting classifier	0.822	0.83	0.85	0.84	0.81	0.78	0.8

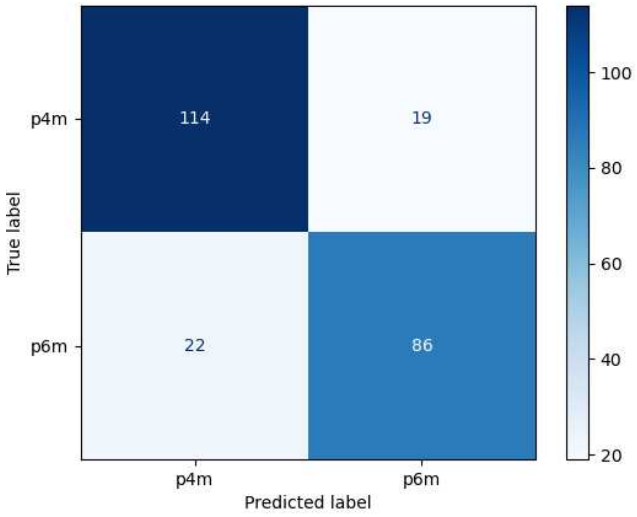

Figure 5. Confusion matrix for the voting classifier

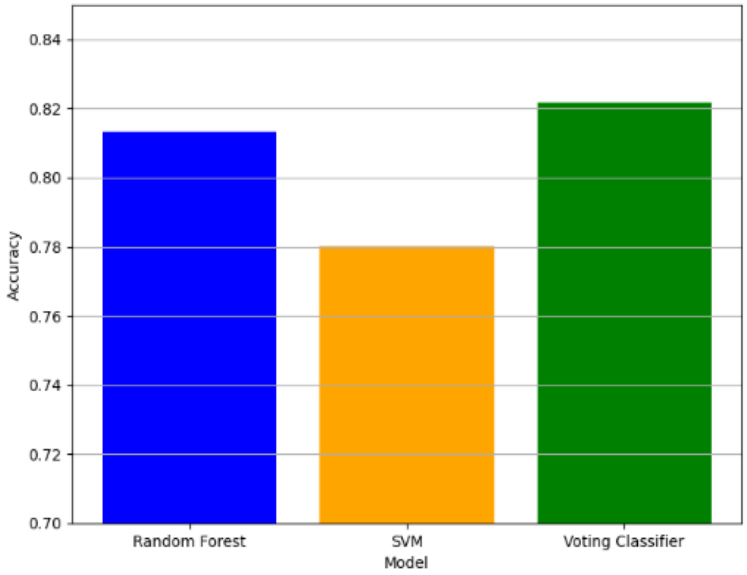

Figure 6. Accuracy comparison across classifiers (RF, SVM, and voting classifier)

4.3. Misclassification analysis

Upon closer examination, misclassifications predominantly arose under three challenging conditions. First, intense Gaussian noise often obscured critical geometric features, complicating the identification of symmetry lines and patterns. This was particularly evident in heavily augmented images, where noise introduced irregularities that moment descriptors struggled to process. Second, extreme rotations distorted the original symmetry of certain p4m and p6m motifs, creating ambiguous patterns that blurred the distinctions between the two classes. Such distortions posed significant challenges for the robustness of the descriptors. Lastly, low contrast in the images led to incomplete or imperfect segmentation, resulting in the loss of key structural details required for accurate feature extraction.

The analysis depicted in Figure 7 provides insights into the error distribution, showing that most misclassifications arise under conditions of noise, extreme rotations, or low contrast, further validating the need for robust preprocessing. By reviewing these outliers, we can pinpoint areas for potential improvement in both preprocessing and the computation of moment descriptors. Addressing these challenges—such as enhancing noise filtering, improving contrast adjustment techniques, or refining the feature extraction pipeline—could further bolster the classifier's performance, especially under adverse conditions.

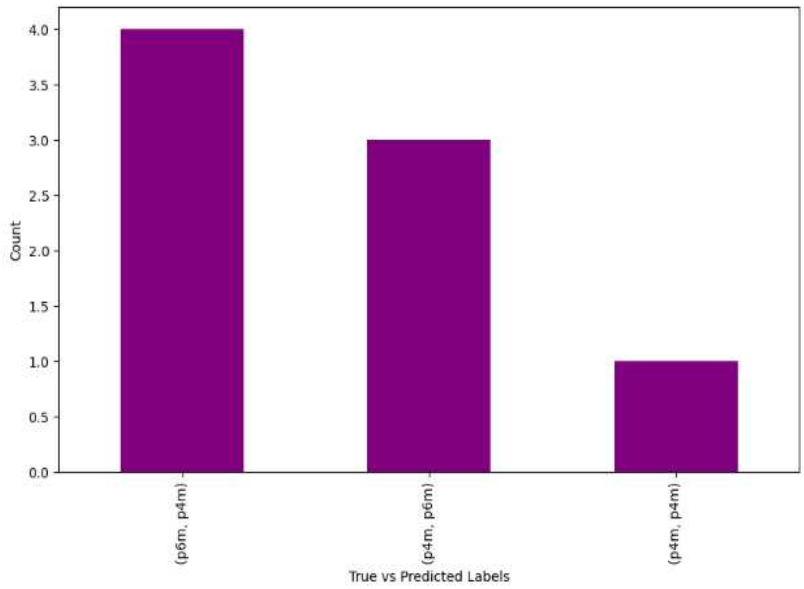

Figure 7. Misclassification analysis illustrating the frequency of errors in classifying p4m and p6m symmetries

5. DISCUSSION

The integration of QCFrHMs provided robust descriptors that significantly improved the classification accuracy of geometric patterns with enhanced robustness against rotations and scaling. QCFrHMs effectively captured fine-grained shape details, especially when integrated with Zernike descriptors, forming a complementary, dual-layer feature representation that encapsulated both global and local structural symmetries. This turned out to be a very effective combination and gave a remarkable accuracy for the differentiation of the classes p4m and p6m, reaching even 82.2% with the voting classifier. The ensemble model capitalized on the strengths of RF and SVM, wherein RF provided stability by variance reduction through bagging, whereas SVM ensured robust margin-based classification in high-dimensional spaces. This synergy thus created a situation where the weaknesses of individual models were offset, their strengths consolidated to provide performance uniformly across diverse conditions.

Despite all these advances, some of the methodological limitations appear. Computing higher-order moments of the fractional order proves computationally expensive for very large datasets, and though median filtering was performed, parts of the residual noise may compromise the precision of the moment-based descriptors. While Gaussian noise, rotation, and scaling enhanced the robustness, other real-world complexities, such as variable lighting or occlusions, may not be fully captured by these augmentations. Comparing these results with the existing literature where Zernike Moments have been widely lauded for shape classification, our approach represents a quantum leap by introducing QCFrHMs that offer enhanced resilience and flexibility.

What is more, this embedding of ensemble learning is on trend according to modern tendencies in classification; this once again underlined its capability for enhancing the accuracy and stability over single models. These results proved that the QCFrHMs are robust and, even more important, the ensemble strategy effectively worked to advance the state-of-the-art in the geometric pattern classification, opening a very firm ground for the applications into cultural heritage preservation and automation of design.

6. CONCLUSION

This research has underscored the effectiveness of combining ensemble learning with advanced moment-based descriptors particularly quaternion cartesian fractional Hahn moments (QCFrHMs) and Zernike moments to classify geometric motifs exhibiting p4m and p6m symmetries. By integrating both descriptor sets, critical geometric traits are more comprehensively captured, while dimensionality reduction via PCA maintains a balance between complexity and accuracy by retaining components covering 95% of the variance. Among the classifiers tested, the voting classifier composed of a RF and an SVM outperforms standalone models, highlighting the advantage of merging complementary algorithms. Although the current results are promising, future work can focus on mitigating computational overhead, enhancing noise resilience, and extending the framework to additional symmetry types or real-time applications. By blending

fractional Hahn polynomial theory with modern ensemble methods, this research opens new pathways in shape analysis and promises wide-ranging applications in computer vision, from industrial quality control to the digital exploration of elaborate ornamental art. Real-time implementation could leverage GPU acceleration and approximate sampling techniques; multi-class symmetry classification could explore additional symmetry groups (p2, p3, p4, p4g, and p6) and automated motif detection in complex images; and deep-learning-based expansions, such as transfer learning or feature fusion with QCFrHMs and Zernike Moments, might produce even more robust, efficient, and precise classification methods.

REFERENCES

[1] F. Mangini, L. Dinia, M. Del Muto, E. Federici, L. Rivaroli, and F. Frezza, "Study of optical tag profile of the tag recognition measurement system in cultural heritage," *Journal of Cultural Heritage*, vol. 45, pp. 240–248, Sep. 2020, doi: 10.1016/j.culher.2020.04.012.

[2] A. Khamjane and R. Benslimane, "A computerized method for generating Islamic star patterns," *Computer-Aided Design*, vol. 97, pp. 15–26, Apr. 2018, doi: 10.1016/j.cad.2017.11.002.

[3] A. Khamjane and R. Benslimane, "Generating Islamic quasi-periodic patterns: a new method," *Journal on Computing and Cultural Heritage*, vol. 11, no. 3, pp. 1–18, Aug. 2018, doi: 10.1145/3127090.

[4] A. Khamjane, Z. Ouazene, A. Taime, I. Badi, K. El Fazazy, and R. Benslimane, "The polygonal technique for constructing Islamic geometric patterns," in *Digital Technologies and Applications*, Springer Nature Switzerland, 2023, pp. 521–530, doi: 10.1007/978-3-031-29860-8_53.

[5] Z. Ouazene, R. Benslimane, and A. Khamjane, "CAD geometry for the traditional Tastir style Moroccan and Andalusian 16-fold rosettes," *Symmetry: Culture and Science*, vol. 33, no. 1, pp. 55–68, 2022, doi: 10.26830/symmetry_2022_1_055.

[6] Z. Ouazene, A. Khamjane, and R. Benslimane, "Relationship between eight-fold star and other tiles in traditional method 'Tastir,'" in *Advanced Technologies for Humanity*, Springer International Publishing, 2022, pp. 352–358, doi: 10.1007/978-3-030-94188-8_33.

[7] A. Khamjane, A. Taime, Z. Ouazene, and R. Benslimane, "Computer graphics for generating Islamic geometric periodic and quasi-periodic patterns," in *2019 International Conference on Intelligent Systems and Advanced Computing Sciences (ISACS)*, Dec. 2019, pp. 1–6, doi: 10.1109/isacs48493.2019.9068879.

[8] A. Khamjane, R. Benslimane, and Z. Ouazene, "Method of construction of decagonal self-similar patterns," *Nexus Network Journal*, vol. 22, no. 2, pp. 507–520, Sep. 2019, doi: 10.1007/s00004-019-00461-4.

[9] Z. Ouazene, "Quasi-periodic tiling in Moroccan and Andalusian decorative art: A harmonious symphony of mathematics and aesthetics," in *Civil Engineering, Material and Smart Buildings: New Technologies in Cities' Infrastructures*, Springer Nature Switzerland, 2024, pp. 22–37, doi: 10.1007/978-3-031-76557-5_3.

[10] A. P. Dzyuba, P. A. Khorin, P. G. Serafimovich, and S. N. Khonina, "Wavefront aberrations recognition study based on multi-channel spatial filter matched with basis Zernike functions and convolutional neural network with Xception architecture," *Optical Memory and Neural Networks*, vol. 33, no. S1, pp. S53–S64, Dec. 2024, doi: 10.3103/s1060992x24700309.

[11] G. Larbi, "Two-step text detection framework in natural scenes based on Pseudo-Zernike moments and CNN," *Multimedia Tools and Applications*, vol. 82, no. 7, pp. 10595–10616, Sep. 2022, doi: 10.1007/s11042-022-13690-6.

[12] B. He, J. Liu, T. Yang, B. Xiao, and Y. Peng, "Quaternion fractional-order color orthogonal moment-based image representation and recognition," *EURASIP Journal on Image and Video Processing*, vol. 2021, no. 1, May 2021, doi: 10.1186/s13640-021-00553-7.

[13] M. Ahadian and A. Bastanfard, "Classification of Islamic geometric pattern images using Zernike moments," in *2011 Eighth International Conference Computer Graphics, Imaging and Visualization*, Aug. 2011, pp. 19–24, doi: 10.1109/cgiv.2011.11.

[14] M. R. Teague, "Image analysis via the general theory of moments*," *Journal of the Optical Society of America*, vol. 70, no. 8, p. 920, Aug. 1980, doi: 10.1364/josa.70.000920.

[15] M. Yamni, H. Karmouni, M. Sayyouri, and H. Qjidaa, "Quaternion cartesian fractional Hahn moments for color image analysis," *Multimedia Tools and Applications*, vol. 81, no. 1, pp. 737–758, Sep. 2021, doi: 10.1007/s11042-021-11432-8.

[16] N. M. Atakishiyev and S. K. Suslov, "The Hahn and Meixner polynomials of an imaginary argument and some of their applications," *Journal of Physics A: Mathematical and General*, vol. 18, no. 10, pp. 1583–1596, Jul. 1985, doi: 10.1088/0305-4470/18/10/014.

[17] C. Huang, J. Li, and G. Gao, "Review of quaternion-based color image processing methods," *Mathematics*, vol. 11, no. 9, p. 2056, Apr. 2023, doi: 10.3390/math11092056.

[18] A. Khotanzad and Y. H. Hong, "Invariant image recognition by Zernike moments," *IEEE Transactions on Pattern Analysis and Machine Intelligence*, vol. 12, no. 5, pp. 489–497, May 1990, doi: 10.1109/34.55109.

[19] S. A. Ramadayanti and A. Prahara, "Classification of tiles using convolutional neural network," *Mobile and Forensics*, vol. 3, no. 2, pp. 58–65, Sep. 2021, doi: 10.12928/mf.v3i2.5643.

[20] M. Cosovic and R. Jankovic, "CNN classification of the cultural heritage images," in *2020 19th International Symposium INFOTEH-JAHORINA (INFOTEH)*, Mar. 2020, pp. 1–6, doi: 10.1109/infoteh48170.2020.9066300.

[21] M. Casillo, F. Colace, R. Gaeta, A. Lorusso, D. Santaniello, and C. Valentino, "Revolutionizing cultural heritage preservation: an innovative IoT-based framework for protecting historical buildings," *Evolutionary Intelligence*, vol. 17, no. 5–6, pp. 3815–3831, Jun. 2024, doi: 10.1007/s12065-024-00959-y.

[22] Y.-J. Cao *et al.*, "Recent advances of generative adversarial networks in computer vision," *IEEE Access*, vol. 7, pp. 14985–15006, 2019, doi: 10.1109/access.2018.2886814.

[23] T. Sun, "3D Gaussian geometric moment invariants," *Applied Artificial Intelligence*, vol. 38, no. 1, Feb. 2024, doi: 10.1080/08839514.2024.2318983.

[24] N. Canterakis, "3D Zernike moments and Zernike affine invariants for 3D image analysis and recognition," *In 11th Scandinavian Conf. on Image Analysis*, vol. In 11th Sc, pp. 85–93, 1999, [Online]. Available: http://ukpmc.ac.uk/abstract/CIT/504643

[25] A. Tahmasbi, F. Saki, and S. B. Shokouhi, "Classification of benign and malignant masses based on Zernike moments," *Computers in Biology and Medicine*, vol. 41, no. 8, pp. 726–735, Aug. 2011, doi: 10.1016/j.compbiomed.2011.06.009.

[26] I. T. Jolliffe, "Principal component analysis and factor analysis," in *Principal Component Analysis*, Springer New York, 1986, pp. 115–128, doi: 10.1007/978-1-4757-1904-8_7.

[27] M. Wattenberg, F. Viégas, and I. Johnson, "How to use t-SNE effectively," *Distill*, vol. 1, no. 10, Oct. 2016, doi: 10.23915/distill.00002.

BIOGRAPHIES OF AUTHORS

Zouhair Ouazene born in Fez, Morocco, in 1986. He held a master's degree in computer graphics and imagery in 2010 and a Ph.D. in computer science in 2022 from the same university. His research focuses on computer graphics, geometry, and art, aiming to create computational tools for ornamental design. He is also active in AI research, particularly in smart agriculture, and recommender systems. He can be contacted at email: zouhair.ouazene@usmba.ac.ma.

Aziz Khamjane born in Fez, Morocco, in 1986, is an Associate Professor of Computer Science at the Multidisciplinary Faculty of Taza, Sidi Mohamed Ben Abdellah University. He earned a master's degree in computer graphics and imagery in 2012 and a Ph.D. in computer science in 2018 from the same university. From November 2019 to April 2025, he was an assistant professor at Abdelmalek Essaadi University and a member of the Laboratory of Applied Sciences at ENSA Al-Hoceima. His research focuses on computer graphics, geometry, and art, aiming to create computational tools for ornamental design. He is also active in AI research, particularly in medical imaging, smart agriculture, and recommender systems. He can be contacted at email: aziz.khamjane@usmba.ac.ma.